11th International Symposium on Turbulence and Shear Flow Phenomena (TSFP11)
Southampton, UK, July 30 to August 2, 2019

LARGE-SCALE STRUCTURES IN TURBULENT BOUNDARY LAYERS UNDER AN ADVERSE PRESSURE GRADIENT UP TO FLOW SEPARATION

Felix Eich, Christian J. Kähler
Institute of Fluid Mechanics and Aerodynamics
Universität der Bundeswehr München
Werner-Heisenberg-Weg 39
85577 Neubiberg, Germany
Felix.Eich@unibw.de

ABSTRACT

The investigation of large-scale coherent structures in turbulent boundary layers has become an established field of research in the last decades. Most studies considered the canonical zero pressure gradient (ZPG) boundary layer flow case. Within this study, a turbulent boundary layer under the impact of a strong adverse pressure gradient up to separation is investigated experimentally up to $Re_\tau = 12000$.

The analysis of the acquired PIV velocity fields shows a persistence of large-scale coherent structures from the preceding zero pressure gradient section through the adverse pressure gradient region until the flow separation takes place. Furthermore, the interaction between the coherent turbulent structures and the flow separation is characterised. Using conditional comparison of mean flow parameters, it is shown that high-momentum structures are able to shift the point of separation downstream while the opposite is true for low-momentum large-scale structures. This interaction has a significant impact on the dynamics of the separation line. It is also demonstrated that the separated region does not have a major influence on the mean boundary layer thickness but the mean flow velocity and spatial scales of coherent structures are visibly influenced.

Introduction

The investigation of large-scale coherent structures in turbulent boundary layers has become an established field of research in the last decades (Marusic *et al.*, 2010; Wallace, 2012). It is well known that the length of the large-scale structures exceed multiple boundary layer thicknesses δ in stream-wise direction and the higher the Reynolds number is the more energetic the structures become. Consequently, researchers try to analyse the structures at large Reynolds numbers to be able to better sample the details of the structures. Unfortunately, the investigation of the large-scale structures is challenging at large Reynolds numbers due to the required spatial resolution and the range of scales that must be resolved.

Most previous studies focused on the canonical zero pressure gradient (ZPG) boundary layer flow case. However, in this work we will focus on an adverse pressure gradient (APG) boundary layer flow for two reasons: First, the intensity of the large-scale structures is increasing with APG making this investigation more reliable even at large Reynolds numbers. Second, we will study the impact of large-scale structures on separated regions and to characterise the interaction. Krogstad & Skåre (1995) showed that turbulent boundary layers under an adverse pressure gradient (APG) are structurally different in many aspects from ZPG boundary layers. In flows with large positive stream-wise pressure gradients $\mathrm{d}p/\mathrm{d}x > 0$ but without flow separation, the known similarity laws and scaling are not applicable (Skåre & Krogstad, 1994; Maciel *et al.*, 2018). Furthermore, Harun *et al.* (2013) observed in pre-multiplied energy spectra an amplification of the energy accumulated in the large-scale structures with increasing pressure gradient. Hence, it is assumed that large-scale structures become a physically more important feature of the flow under an APG. Maciel *et al.* (2018) made similar observations in different data sets. They concluded that the near wall region becomes less important with increasing APG because the turbulence activity and production is moved further away from the wall, towards the region where large-scale structures exist. Consequently it seems likely that APG boundary layers allow to study the physics of large-scale structures more reliably.

If the pressure gradient is further increased, the boundary layer flow separates. As the large-scale structures are associated with a large amount of turbulent kinetic energy, it is of interest to examine how the separation itself is affected by the presence of large-scale structures in the flow and how the large-scale structures behave when interacting with the separated region. Many previous studies investigating separation focused on flows, e.g. over airfoils, or geometry induced flow separation. Elyasi & Ghaemi (2019) showed using PIV and Tomographic-PIV that three dimensional flow fields including large-scale structures occur in the vicinity of a flow separation.

The aim of this study is to investigate the effect of strong APG conditions on large-scale structures in turbulent boundary layers in comparison to structures in canonical ZPG boundary layers and to resolve the interaction between large-scale structures and the separated flow regions. Therefore, turbulent boundary layer measurements were performed in the Atmospheric Wind Tunnel Munich (AWM) at a Reynolds number range of $Re_{\tau,\mathrm{ZPG}} = 8400 - 12000$. The Reynolds number is calculated under ZPG conditions as a reference, because the viscous scaling is not applicable under strong APG conditions and separated flows (Maciel

et al., 2018). In the following, the coordinates x, y and z correspond to stream-wise, wall-normal and span-wise directions, u, v and w to the respective velocity components. To differentiate between the absolute wind tunnel fixed x, y, z-coordinate system and the coordinate system of a specific measurement set-up over the boundary layer, a relative x^*, y^*, z^*-coordinate system, with $x^* = x - x_0$, which is the coordinate parallel to the wall with its origin $x^* = 0$ at the centre of the corresponding measurement x_0, is used. Temporally averaged values are indicated with an overbar ($\overline{\phi}$), fluctuations with a dash (ϕ'), conditional averaged values with brackets ($\langle\phi\rangle$) . The superscript "+" refers to viscous scaled units.

Experimental Systems and Methods

The experiments analysed in this study were conducted in the Atmospheric Wind Tunnel Munich (AWM), which is an Eiffel type wind tunnel with a 22 m long test section and a cross-section area of 1.85 m × 1.85 m. This enables measurements of a fully developed boundary layer without influence of the opposite wind tunnel wall or corner vortices (Jones *et al.*, 1995). To achieve a pressure gradient distribution, two different turbulent boundary layer models, each consisting of two S-shaped flow deflections, are installed in the wind tunnel side wall. In between the flow deflections, a 4 m long flat plate is installed over which zero pressure gradient conditions are present. At the decelerating downstream flow deflection, the flow is subject to a well defined adverse pressure gradient (APG). While for the first boundary layer model, fully attached turbulent boundary layers are studied, the second model is shifted further into the wind tunnel centre and the contour angle of the straight APG section is increased from 14° to 18° relative to the wind tunnel centre line. This results in a longer APG impact and finally in flow separation. The boundary layer model 2 ends in a sharp corner at $x = 0$ m to stabilise the separated flow region. In figure 1, the downstream end of the boundary layer model contours with the resulting pressure gradient distributions $\mathrm{d}p/\mathrm{d}x$ are plotted for both models and investigated Reynolds numbers. An overview of the flow parameters over both models at the tested Reynolds numbers is given in table 1

The data was acquired using standard 2D2C PIV and stereo 2D3C PIV (SPIV) measurements in wall-parallel (x^*z^*), wall-normal (x^*y^*) (APG only) and cross-stream (y^*z^*) planes. Multiple PCO.edge 5.5 sCMOS cameras with a sensor size of 2560 × 2160 pixel were used in side by side arrangements to capture a sufficient large field of view (FOV). This is necessary to analyse large-scale coherent structures in their full spatial extent, with sufficient spatial resolution and accuracy. The illumination was provided with a Spectra Physics Quanta-Ray PIV Nd:YAG laser for the x^*z^*-plane measurements and with an Innolas SpitLight 400 Compact Nd:YAG laser for all other measurements. Tracer particles were generated from two Laskin nozzle seeders using Di-Ethyl-Hexyl-Sebacat (DEHS) as aerosol, which results in particles with a mean diameter of 1 μm (Kähler *et al.*, 2002).

Vector fields were computed from the acquired particle images with the commercial PIV software DaVis from LaVision. Using a multi-pass PIV algorithm with 50 % interrogation window overlap, vector fields with vector spacings of 1 mm − 2.7 mm were achieved. Details on the PIV evaluation techniques can be found in Raffel *et al.* (2018). The individual vector fields were stitched together using Matlab to a single flow field for processing and visualisation, which results in the large fields presented in this paper.

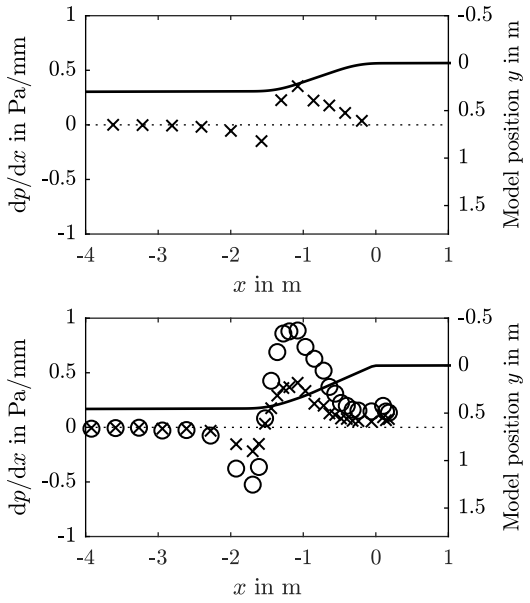

Figure 1. Pressure gradient distribution $\mathrm{d}p/\mathrm{d}x$ over the boundary layer models. Symbols correspond to different Reynolds numbers. Top: Model 1 × : $Re_\tau = 9300$. Bottom: ○ : $Re_\tau = 12000$, × : $Re_\tau = 8400$. The solid line represents the model contours.

Results

In the following sections, the results will be presented and discussed, focusing on the impact of an APG on the boundary layer itself and the contained large-scale structures.

Comparison between APG and ZPG boundary layer

The most intuitive approach to get an impression of the structural pattern of a boundary layer flow is the visual inspection of instantaneous flow fields after subtracting the local mean velocity. In figure 2, the spatial distribution of instantaneous normalised velocity fluctuations $u'/\overline{u}$ in stream-wise direction are plotted for ZPG flow and an attached APG flow in a wall-parallel x^*z^*-plane. Large elongated structures with positive (red) and negative (blue) momentum relative to the mean motion are found in both measurements. In the span-wise direction, the structures align in a streaky topology side by side, which is in accordance with the results from Hutchins & Marusic (2007b). Due to the lower spatial resolution of the measurements, the ZPG flow fields appear slightly smoother in comparison to the APG flow fields. Observing the same structural pattern under ZPG as well as APG flow conditions shows that large-scale structures are also dominant under the APG flow conditions. The relative fluctuations are measured to be higher under an APG, which confirms the increase in large-scale energy under an APG (Harun *et al.*, 2013).

It should be noted that observing a wall-parallel plane is not an observation at a constant wall distance y^*/δ_{99} in the APG case, as the increase in boundary layer thickness is

Table 1. Flow parameters over the models.

Case	$Re_{\tau,\mathrm{ZPG}}$	$u_{\tau,\mathrm{ZPG}}$	$\delta_{99,\mathrm{ZPG}}$	$1/y^+$	$\delta_{99,\mathrm{APG}}$	β	$x_{0,\mathrm{ZPG}}$	$x_{0,\mathrm{APG}}$
		m/s	m	μm	m		m	m
Model 1	9300	0.98	0.148	15.1	0.22	21	-3.3	-0.45
Model 2	8400	1.11	0.112	14.0	0.24	x	-3.8	-0.34
Model 2	12000	1.67	0.107	9.2	0.24	x	-3.8	-0.34

significantly large under APG impact. The given number is calculated in the centre of the image. For the ZPG case the increase of the boundary layer thickness is $< 0.3\%$ of δ_{99} within the cropped field of view of $1 \times 2.1\delta_{99}$ in figure 2. Hence, the plane can be considered as wall parallel also in a relative sense. The decrease of relative wall distance for the APG flow field in combination with an overall decreasing mean velocity under APG impact explains the increase of relative fluctuations from upstream to downstream in the measured flow field. Details on the resulting spatial scales such as length, width and and periodicity in comparison between ZPG and APG can be found in Eich & Kähler (2017).

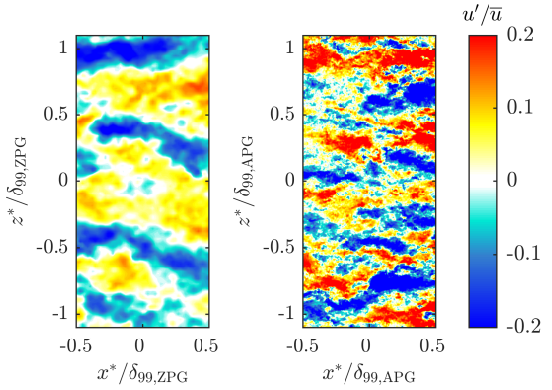

Figure 2. Instantaneous stream-wise velocity fluctuations $u'/\overline{u}$ in wall parallel planes $y^*/\delta_{99} = 0.14$ and Reynolds number $Re_{\tau,\mathrm{ZPG}} = 9300$. Left: ZPG flow; right: APG flow.

Analysis of the structural pattern

To examine the corresponding structural pattern, the flow fields in the APG close to the separation were analysed by means of two-point correlations. In figure 3, exemplary correlation function are shown for the APG flow at $Re_{\tau,\mathrm{ZPG}} = 12000$ for three different wall-normal positions and two stream-wise positions. The red correlation functions are close to the edge of the boundary layer, the blue ones are within the large-scale structure dominated region and the black correlation functions are in the vicinity of the separated region. The shape of the positive correlated region outside the separated region is qualitatively similar to ZPG flow (Buchmann *et al.*, 2016). Characteristic is the elongated shape inclined to the wall. The shape of the correlation function is mainly dependent on the wall-normal location.

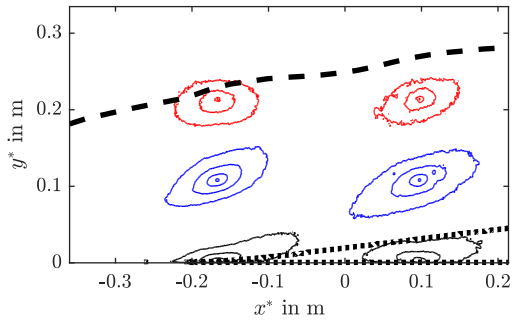

Figure 3. Two-point correlation function $R_{u'u'}$ at three different wall normal locations and two stream-wise positions. Contour lines are drawn at $R_{u'u'} = 0.3,\ 0.5,\ 0.7$ and 0.9. The dashed line $(--)$ corresponds to the average boundary layer thickness δ_{99}, the dotted line $(\cdot\cdot)$ to the average separated region.

While the correlation functions close to the edge of the boundary layer reveals a round shape as a result of intermittency effects (Reuther & Kähler, 2019), the blue correlation functions are elongated in stream-wise direction due to the presence of large-scale structures. The black correlation is dominated by the separation. Clearly visible is the change between the correlation at $x^* = -0.18\,\mathrm{m}$ upstream of the separated region and $x^* = 0.1\,\mathrm{m}$ within the separated region.

Based on the correlation functions, characteristic values can be calculated, such as the length L_2 in a cut plane of the correlation function and the angle α relative to the wall. The resulting scales are plotted in figure 4. The length scale L_2 is calculated using a threshold for the correlation of the stream-wise fluctuation of $R_{u'u'} = 0.3$. The correlated length at a comparable ZPG position is $L_{2,\mathrm{ZPG}} = 1.9 \cdot \delta_{99}$ at $y^*/\delta_{99} = 0.14$. Normalisation is made with the ZPG boundary layer thickness $\delta_{99,\mathrm{ZPG}}$ to have a similar scaling of all positions within the field of view and flow cases. The high value of $R_{u'u'} = 0.3$ as chosen threshold is necessary to ensure that the correlation function is within the field of view for the chosen value to calculate the length scales over the field of view. The correlated structure length in the outer APG boundary layer is $L_2 \approx 1.1\delta_{99,\mathrm{ZPG}}$, hence $\approx 40\%$ shorter than in the ZPG case. This effect is a result of the impact of the APG, which shortens the structures due to the deceleration of the flow in this region, as also shown by Harun *et al.* (2013) in hot wire data and Hain *et al.* (2016) in PIV data.

Interestingly, in the vicinity of the separated region the correlated length scales increase. Two different effects must be considered there: First, the separated region is highly un-

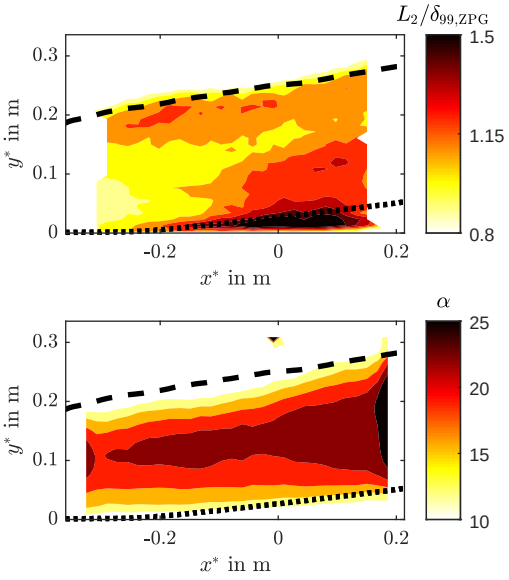

Figure 4. Evolution of the structure length L_2 (top) and structure angle α (bottom) under APG conditions calculated from two-point correlation functions at $Re_{\tau,\mathrm{ZPG}} = 8400$. Dashed line $(--)$ corresponds to the average boundary layer thickness δ_{99}, the dotted line $(\cdot\cdot)$ to the average separated region.

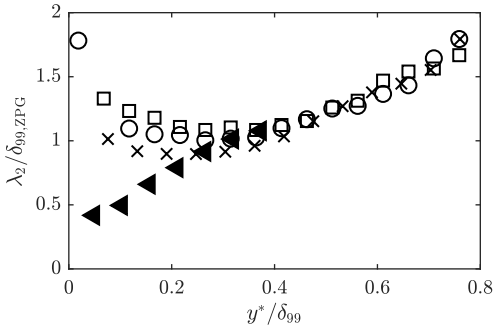

Figure 5. Span-wise spacing λ_2 of large-scale structures under APG with flow separation. The filled symbols (◀) represent the reference case without flow separation at $Re_{\tau,\mathrm{ZPG}} = 9300$ over model 1. The other symbols correspond to different stream-wise positions of the measurement at $Re_{\tau,\mathrm{ZPG}} = 12000$ at model 2. $\times$: $x^* = -0.18\,\mathrm{m}$; $\circ$: $x^* = 0\,\mathrm{m}$ and $\square$: $x_0 = 0.18\,\mathrm{m}$.

steady due to the action of the large-scale structures, hence its spatial extent is in multiple fields larger than on average. As the fluctuation signal in the separated region is similar compared to the flow outside the separation, the separated region correlates positive, which bias's the calculated spatial scales of the turbulent structures. This explains the dark area in figure 4 top with length scales of $L_2 = 1.5\delta_{99,\mathrm{ZPG}}$ directly above the average separated region. The second effect is the increase of length above the separated region, which can be interpreted as a stretching of large-scale structures when convecting directly over an obstacle like a separation.

Also significant is the change in the angle of the correlated structure relative to the wall, as shown in figure 4 bottom. The angle was calculated for the $R_{u'u'} = 0.3$ correlation line. While for ZPG flow, characteristic angles of $\approx 7 - 15^\circ$ are observed depending on the wall position y (Adrian *et al.*, 2000; Buchmann *et al.*, 2016), this angle is increased up to $> 20^\circ$ due to the APG and beginning flow separation. Kitsios *et al.* (2017) made comparable observations in a direct numerical simulation at smaller Reynolds numbers. They observed an increase from $\alpha = 7^\circ$ under ZPG to $\alpha = 27^\circ$ for strong APG conditions. In addition, an increase of the correlated structure angle in downstream direction is present, which is due to an increase of the exposure time to an APG.

Besides the scaling of the structures in stream-wise direction, the span-wise pattern is analysed. As shown in figure 2, a characteristic intermittent pattern of high and low momentum structures is present in ZPG as well as APG. To characterise this pattern, the spacing λ_2 in a wall-parallel cut plane is calculated form two-point correlations and plotted in figure 5. The solid symbols correspond to an attached APG flow at $Re_{\tau,\mathrm{ZPG}} = 9300$, the other symbols to different stream-wise locations of the flow case with a separation present at $Re_{\tau,\mathrm{ZPG}} = 12000$. The calculated structures spacings for the cases with a separation are larger up to wall distance $y^*/\delta_{99} = 0.35$. This is the effect of the separation. Above, the spacings follow the similar trend as the attached APG. Those results are in line with the previous observations that the separated region mainly effects the flow in its close proximity, but large-scale structures as energetic features are persistent.

Analysis of a separated turbulent boundary layer

To characterise the effect of large-scale structures on the flow separation it is necessary to quantify the unsteadiness of the separation itself and the effect of the separation dynamics on characteristic boundary layer parameters. In figure 6 left, a cumulative distribution function P of the separation location $x^*_{u<0}$ is shown. The separation location is defined as the position of the first area with negative flow velocity, which includes more than 150 vectors. This enables an instantaneous detection, because the common approach for separation detection via the wall-normal velocity gradient is uncertain within the PIV fields due to turbulent noise and measurement uncertainty near the wall, where small pixel displacements occur. The number of $N = 150$ connected vectors is chosen based on the observations in instantaneous flow fields, where small prior separations occur before the flow is completely separated. Sensitivity analysis of the chosen threshold number N showed no changes in the qualitative observations and conclusion, only the absolute separation location changes.

The results show that the separation location is strongly unsteady. Furthermore, clear influence of the Reynolds number is detectable. The higher the Reynolds number and thereby the free stream velocity and mean momentum, the later the flow separates. Furthermore, the stream-wise domain were the unsteadiness of the separation takes places shrinks with the Reynolds number.

To analyse the corresponding flow fields, the data is conditioned into five quantiles, depending on the location of the flow separation in the instantaneous flow field. Quantile one represents the most upstream separation locations, continuing downstream. While no effect on the boundary layer thickness δ_{99} is present, a clear influence on various boundary layer parameters such as the shape factor H, displacement thickness and the momentum thickness θ was

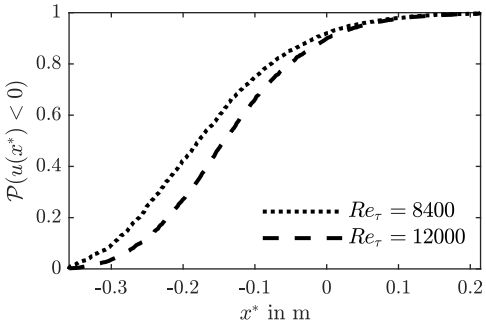

Figure 6. Cumulative distribution function $P(u(x^*) < 0)$ of the instantaneous separation starting position for different Reynolds numbers.

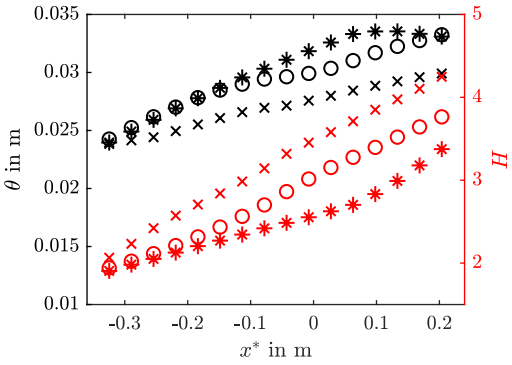

Figure 7. Comparison of the momentum loss thickness θ and shape factor H for the first quintile $\times$, fifth quintile $*$ and all data $\circ$.

detected, as shown in figure 7 for quintiles 1, 5 and the complete data set. The later the separation occurs, the smaller the momentum thickness becomes. The shape factor H is increasing from $H = 1.9$ at the upstream end of the field of view to $H \approx 4$ at the downstream end where the flow is separated, as is expected for an increasing APG (Maciel *et al.*, 2017). In comparison, the shape factor is $H = 1.4$ for a ZPG TBL, the higher shape factors highlight that the mean profile is subject to increasing deceleration near the wall. Also a characteristic change of slope of the shape factor occurs near the average separation location of the analysed quintile, hence the shape factor can also be used as a detection criterion for the separation location.

Besides the average parameters of the TBL, the influence of the separation location on the velocity field is evaluated. In figure 8, the difference between conditioned mean velocities of quintiles 1 (top) and 5 (bottom), $\langle u_i \rangle$, and the overall mean $\overline{u}$ is plotted. On average, the flow velocity is lower for the further upstream separation location, while for the downstream separation location the opposite is the case. The dotted line marks the corresponding ensemble average of the separated region of the plotted quintile. These dynamics of the separated region can be explained with the impact of large-scale structures on the separation itself, as qualitatively shown in the sketch in figure 9. High momentum large-scale structures push the separation line downstream, whereas low momentums large-scale structures favour flow separation. This is possible because the turbulent large-scale structures alter the flow dynamics down to the

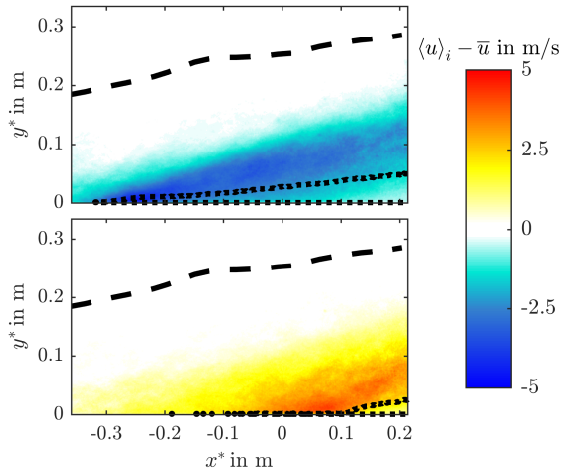

Figure 8. Conditioned stream-wise mean velocity $\langle u_i \rangle$ in comparison to the average mean velocity field $\overline{u}$ at $Re_\tau = 12000$. Top: Upstream flow separation location (quintile 1). Bottom: Downstream flow separation location (quintile 5). Dashed line $(- -)$ corresponds to the average boundary layer thickness δ_{99}, the dotted line $(\cdot\cdot)$ to the average separated region.

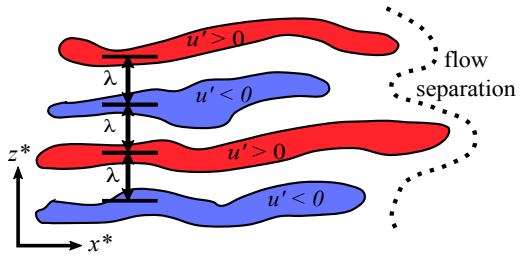

Figure 9. Sketch of the large-scale structure impact on the position of the flow separation.

wall (Bross *et al.*, 2019).

The dashed line in figure 8 corresponds to the average boundary layer thickness δ_{99} of the plotted quintiles. As stated before, no differences are found for the five investigated separation locations. This observation is in accordance with the displayed differences of the mean velocity. The faster and slower mean velocities only extend up to $y^*/\delta_{99} \approx 0.6$ in maximum, hence the outer boundary layer flow is unaffected by the unsteady separation. This highlights that the interaction between flow and separation only takes place in the inner boundary layer where large-scale structures are present. Furthermore, this proves that the unsteadiness is not an effect of changes of the wind tunnel inflow velocity, because this would also effect the outer boundary layer as well, but an effect of turbulent large-scale structures.

Conclusions

Within this study an adverse pressure gradient turbulent boundary layer flow with flow separation was investigated experimentally at Re_τ up to 12000 using optical measurement techniques.

Two-point correlation shows that the structural pattern

does not change significantly with pressure gradients. This shows that large-scale structures keep their structural features until they interact with the separated region. The streamwise length of the correlation is decreasing due to flow declaration. Besides, the inclination relative to wall increases up to $\alpha = 25°$. In contrast to the length, the span-wise spacing of the structures is unaffected by the APG. Only in the direct vicinity of the separated region, the span-wise scales change.

The unsteadiness of the flow separation front was shown to be related to the action of turbulent large-scale structures. In effect the mean boundary parameters are also partly determined by the topology and dynamics of large-scale structures. While no influence on the boundary layer thickness δ_{99} could be found, the displacement and momentum thickness and thereby the shape factor change and can be used to quantify the state of the boundary layer flow.

Furthermore, conditioned flow analysis showed an interaction between the large-scale structures and the separated region, which takes place in the inner boundary layer up to $y^*/\delta_{99} < 0.6$. The separation location and the dynamic of the separation is dependant on the stream-wise momentum of the large-scale structures. The outer flow is unchanged by the unsteady separated region. These observation makes it possible to better understand the dynamics of pressure induced flow separations.

REFERENCES

Adrian, R. J., Meinhart, C. D. & Tomkins, C. D. 2000 Vortex organization in the outer region of the turbulent boundary layer. *Journal of Fluid Mechanics* **422**, 1–54.

Bross, M., Fuchs, T. & Kähler, C. J. 2019 Interaction of coherent flow structures in adverse pressure gradient turbulent boundary layers. *J. Fluid Mech.* **Accepted for publication**.

Buchmann, N. A., Kücükosman, Y. C., Ehrenfried, K. & Kähler, C. J. 2016 Wall pressure signature in compressible turbulent boundary layers. In *Progress in Wall Turbulence 2*, pp. 93–102. Springer.

Eich, F. & Kähler, C. J. 2017 Towards capturing large scale coherent structures in boundary layers using particle image velocimetry. In *Proceedings of the 10th Turbulence and Shear Flow Phenomena Conference, 06. - 09. July. 2017, Chicago, USA*.

Elyasi, M. & Ghaemi, S. 2019 Experimental investigation of coherent structures of a three-dimensional separated turbulent boundary layer. *Journal of Fluid Mechanics* **859**, 1–32.

Hain, R., Scharnowski, S., Reuther, N.and Kähler, C. J., Schröder, A., Geisler, R., Agocs, J., Röse, A., Novara, M., Stanislas, M. *et al.* 2016 Coherent large scale structures in adverse pressure gradient turbulent boundary layers. In *18th international symposium on the application of laser and imaging techniques to fluid mechanics Lisbon Portugal July 4, 7, 2016*, pp. 474–496.

Harun, Z., Monty, J. P., Mathis, R. & Marusic, I. 2013 Pressure gradient effects on the large-scale structure of turbulent boundary layers. *Journal of Fluid Mechanics* **715**, 477–498.

Hutchins, N. & Marusic, I. 2007b Evidence of very long meandering features in the logarithmic region of turbulent boundary layers. *Journal of Fluid Mechanics* **579**, 1–28.

Jones, M. B., Marusic, I. & Perry, A. E. 1995 The effect of aspect ratio and divergence on the turbulence structure of boundary layers. In *Proc. 12th Australasian Fluid Mech. Conf*, pp. 436–439.

Kähler, C. J., Sammler, B. & Kompenhans, J. 2002 Generation and control of tracer particles for optical flow investigations in air. *Experiments in Fluids* **33** (6), 736–742.

Kitsios, V., Sekimoto, A., Atkinson, C., Sillero, J. A., Borrell, G., Gungor, A. G., Jiménez, J. & Soria, J. 2017 Direct numerical simulation of a self-similar adverse pressure gradient turbulent boundary layer at the verge of separation. *Journal of Fluid Mechanics* **829**, 392–419.

Krogstad, P.-Å. & Skåre, P. E. 1995 Influence of a strong adverse pressure gradient on the turbulent structure in a boundary layer. *Physics of Fluids* **7** (8), 2014–2024.

Maciel, Y., Gungor, A. G. & Simens, M. 2017 Structural differences between small and large momentum-defect turbulent boundary layers. *International Journal of Heat and Fluid Flow* **67**, 95–110.

Maciel, Y., Wei, T., Gungor, A. G. & Simens, M. P. 2018 Outer scales and parameters of adverse-pressure-gradient turbulent boundary layers. *Journal of Fluid Mechanics* **844**, 5–35.

Marusic, I., McKeon, B. J., Monkewitz, P. A., Nagib, H. M., Smits, A. J. & Sreenivasan, K. R. 2010 Wall-bounded turbulent flows at high reynolds numbers: recent advances and key issues. *Physics of Fluids* **22** (6), 065103.

Raffel, M., Willert, C. E., Scarano, F., Kähler, C. J., Wereley, S. T. & Kompenhans, J. 2018 *Particle image velocimetry: a practical guide*. Springer.

Reuther, N. & Kähler, C.J. 2019 Effect of the intermittency on the outer scales in turbulent boundary layers. In *Proceedings of the 11th Turbulence and Shear Flow Phenomena Conference, 30. July - 02. August 2019, Southampton, UK*.

Skåre, P. E. & Krogstad, P.-Å. 1994 A turbulent equilibrium boundary layer near separation. *Journal of Fluid Mechanics* **272**, 319–348.

Wallace, J. M. 2012 Highlights from 50 years of turbulent boundary layer research. *Journal of Turbulence* **13**, N53.